Computers in Biology and Medicine 112 (2019) 103360

Contents lists available at ScienceDirect

Computers in Biology and Medicine

journal homepage: www.elsevier.com/locate/compbiomed

Investigation on distal femoral strength and reconstruction failure following curettage and cementation: In-vitro tests with finite element analyses

Azadeh Ghouchani[a], Gholamreza Rouhi[a,*], Mohammad Hosein Ebrahimzadeh[b]

[a] Faculty of Biomedical Engineering, Amirkabir University of Technology, 424 Hafez Ave, Tehran, Iran
[b] Orthopedic Research Center, Department of Orthopedic Surgery, Mashhad University of Medical Sciences, Ahmad Abad Street. Ghaem Hospital, Mashhad, Iran

ARTICLE INFO

Keywords:
Distal femoral strength
In-vitro compressive tests
Quantitative computed tomography
Failure analysis
Finite element method
Non-homogeneity
Non-linear behavior

ABSTRACT

Cement augmentation following benign bone tumor surgery, i.e. curettage and cementation, is recommended in patients at high risk of fracture. Nonetheless, identifying appropriate cases and devices for augmentation remains debatable. Our goal was to develop a validated biomechanical tool to: predict the post-surgery strength of a femoral bone, assess the precision and accuracy of the predicted strength, and discover the mechanisms of reconstruction failure, with the aim of finding a safe biomechanical fixation. Tumor surgery was mimicked in quantitative-CT (QCT) scanned cadaveric human distal femora, and subsequently tested in compression to measure bone strength (F_{Exp}). Finite element (FE) models considering bone material non-homogeneity and non-linearity were constructed to predict bone strength (F_{FE}). Analyses of contact, damage, and crack initiation at the bone-cement interface (BCI) were completed to investigate critical failure locations. Results of paired t-tests did not show a significant difference between F_{Exp} and F_{FE} ($P > 0.05$); linear regression analysis resulted in good correlation between F_{Exp} and F_{FE} ($R^2 = 0.94$). Evaluation of the models precision using linear regression analysis yielded $R^2 = 0.89$, with the slope = 1.08 and intercept = −324.16 N. FE analyses showed the initiation of damage and crack and a larger cement debonding area at the proximal end and most interior part of BCI, respectively. Therefore, we speculated that devices that reinforce critical failure locations offer the most biomechanical advantage. The QCT-based FE method proved to be a reliable tool to predict distal femoral strength, identify some causes of reconstruction failure, and assist in a safer selection of fixation devices to reduce post-operative fracture risk.

1. Introduction

The distal femur is the most vulnerable site for benign bone tumors, such as a giant cell tumor (GCT) [1]. Curettage and defect reconstruction with bone cement is the procedure of choice for this kind of tumors [2]; however, post-operative fracture is a complication, especially in patients with large defects. A high incidence of post-operative fracture, i.e. up to 25%, in patients with GCT treated with curettage followed by cryosurgery and cement infilling has been reported [3]. In spite of the importance and high rate of fracture, to date, little attention has been paid to the biomechanics of a reconstructed bone or the mechanisms of its fracture [4]. When a surgeon feels the patient is prone to fracture, cement augmentation with internal fixation devices is usually applied [5–7]. Among different fixation devices, plates, screws, and pins with the common configuration shown in Fig. 1 are usually used. However, there is a dearth of a reliable and universally accepted method to identify patients at high risk of fracture following the surgery [4]. Also, the best device for cement augmentation to prophylactic bone stabilization is not yet known [8], possibly due to a poor understanding of the mechanics of the bone-cement interface (BCI), which is the site of the fixation device placement.

Most previous studies regarding post-operative fractures in bone cancer patients are retrospective or in-vitro studies, which by their nature either disregard or underestimate the impact of the mechanics of BCI on the outcome of the reconstruction [9–11]. The finite element method (FEM) has gained wide application in orthopedic biomechanics since it can provide information that would be difficult or even impossible to obtain from experimental or clinical studies [8].

FEM has been extensively used to study the mechanics of the human body's inner structures ranging from investigating bone remodeling under different loading conditions to evaluating various surgery methods [12–20]. However, computational and finite element models used to study bone tumors and metastasis are still in their early stages, although they are becoming more common with advances in modeling

* Corresponding author.
E-mail addresses: aghouchani@aut.ac.ir (A. Ghouchani), grouhi@aut.ac.ir (G. Rouhi), ebrahimzadehmh@mums.ac.ir (M.H. Ebrahimzadeh).

https://doi.org/10.1016/j.compbiomed.2019.103360
Received 22 February 2019; Received in revised form 14 July 2019; Accepted 15 July 2019

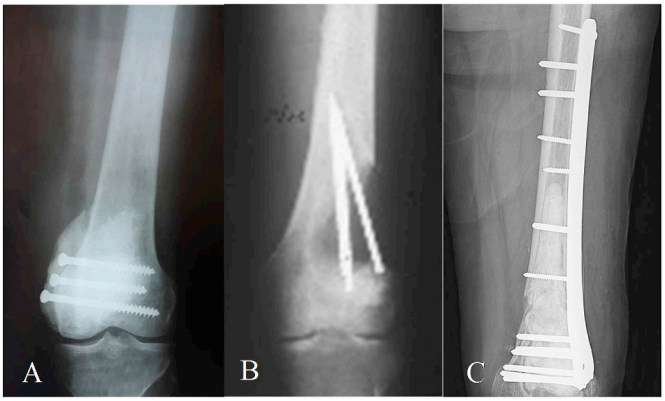

Fig. 1. Common devices used for cement augmentation in distal femoral tumorous defects are: (A) Screws, (B) Intramedullary pins [61], and (C) A plate.

technologies. In 2014 the formation and growth of bone metastatic lesions were studied using computational models, which resulted in reasonable outcomes and fair agreement with in-vivo experiments [21]. In another study, patient specific FE modeling outcomes were compared with experienced clinicians' prediction regarding fractures in a metastatic bone, the study concluded that FEM is a suitable tool to predict the fracture risk for patients who are at high risk of fracture [22]. In 2018, the effect of metastasis size, in healthy and osteoporotic bone, on vertebral height and bulge was investigated using FEM, considering homogeneous and linear material properties for bone and metastatic lesion [23].

Nonetheless, with regard to post-operative fracture risk in patients with bone tumors, most FEM investigations have exclusively concentrated either on determining bone strength following surgery or on selecting the best device for cement augmentation based on bone strength and stiffness, with no focus to the impact of BCI on the outcome [12,24].

Studies on the causes of failure in cemented hip prosthesis have revealed BCI failure or cement debonding from the prosthesis as major sources of prosthesis instability and arthroplasty failure [25–27]. Failure at the BCI might also be the main cause of fracture after cementation following tumor removal [28]. Since the simulation of actual crack initiation and growth is difficult to accomplish utilizing conventional FEM, a recently developed finite element (FE) technique, the eXtended Finite Element Method (XFEM), in which fractures can be simulated without the essence of defining the crack path should be employed [29]. XFEM has already been used in orthopedic biomechanics to investigate the fracture behavior of cortical bone and has shown promising results [30–32]. Notwithstanding the importance of the mechanics of BCI, considering the factors affecting bone strength, as the key determinant of its fracture risk [33], is essential in predicting the risk of a bone fracture. Based on recent studies [34–37], it is known that mechanical load distribution within the bone (which depends on the distribution of mechanical properties, namely the elastic modulus) is an important factor along with bone apparent density and size in determining the bone strength. It is also well known that bone is an inhomogeneous material. This includes both trabecular and cortical bone, each having a very different modulus of elasticity that is not even constant throughout the cortical and trabecular bone regions. Hence, identifying the accurate material properties of bone is necessary if one intends to predict the risk of bone fracture. It is well known that the material properties of a bone depend strongly on its apparent density [33]. Most benign bone tumors, such as GCT, have a distinct geographic border, which means that tumor cells are only present in the tumor zone, and the affected bone is just locally not globally disturbed [38,39]. Even if tumor cells are present throughout a bone, such as in a metastatic bone, it has been shown that this does not affect the relationships between bone density and mechanical properties [22,23,33]. Therefore, relationships between bone density and its material properties derived for an intact bone could be also used for the same bone affected by cancer [22,23,33]. In spite of considering accurate material properties and boundary conditions which mimic the real system, the precision and accuracy of all FE models must be validated before employing the FE model's results in clinical problems or using it in lieu of expensive in-vitro experiments. When validated, the FE models can be used to study the behavior of bones, bone-implant construct, and other tissues under different loading conditions. Previous numerical studies on the outcome of benign bone tumor surgery suffer from the lack of a validation process [24,40].

The purpose of this study was, therefore, to come up with an experimentally validated in-silico tool which can predict the distal femoral fracture risk as well as identify some mechanisms of reconstruction failure following tumor curettage and cementation, with the long-term goal of decreasing the likelihood of re-surgery due to post-operative fractures. A finite element technique, based on quantitative computed tomography (QCT), in which accurate and non-homogeneous distribution of bone material properties was taken into account was used. The accuracy and precision of the models created in this study, i.e. QCT-based FE models, were then evaluated. After validation of the FE models ability to predict bone strength, the mechanisms of reconstruction failure at the BCI were investigated, and based on the FE results suggestions regarding the implant(s) for cement augmentation that may offer the safest biomechanical fixation are provided.

2. Methods and materials

2.1. Experimental part

This study received approval letter (# 1397.768) from the Mashhad University of Medical Sciences institutional review board committee (IRB), in terms of ethical issues for human tissue usage. Therefore, seven pairs of fresh-frozen cadaveric distal femoral human bones were employed. Distal femora bones, as the most persistent site of benign bone tumors, such as GCT involvement, and a very common site of fracture, were used in this study. No musculoskeletal disorders, observable cracks or fracture signs were present in the specimens used in this study. In each pair, a defect simulating tumor curettage was created in one randomly selected specimen by an orthopedic surgeon. The contralateral bone was kept intact to evaluate the FE models ability to predict the strength of both intact and defective bones as compared to their corresponding strengths calculated from experimental tests. The defects were then filled with PMMA bone cement (Biomet Bone Cement R, Zimmer Biomet Co., USA) which was forced by hand to ensure its penetration into the surrounding spongy bone. The anatomical site of the defect involvement was determined by the surgeon and the size of the defects were calculated both in the laboratory by measuring the volume of water poured in the defects and via the tools provided in the modeling software by calculating the regions occupied by the cement. Information about the size and location of the defects created, as well as the donor age and gender is presented in Table 1.

All specimens were separately placed in a container of water to simulate the attenuation of soft tissues and avoid beam hardening effects [37], then scanned using a clinical scanner (Siemens-Somatom 64, 140 kV, 80 mAs, 0.5 × 0.5 mm/pixel resolution, and 1 mm slice thickness). A calibration phantom with five tubes of known densities (Mindways Soft-ware, Inc., San Francisco, CA) was also positioned beneath the container during the scanning process to convert the resulting Hounsfield units (HUs) to bone ash densities (ρ_{ash}).

After scanning, each specimen was positioned in the DTS machine (Dynamic Testing Machine, Hct400/25, Zwick/Roell) with the bone diaphysis aligned with the z-direction and parallel to the machine cylinder that applied compressive load on the medial condyle which was also in the bone longitudinal direction (Fig. 2). The axial force, as an

Table 1
Data related to geometric properties of defects created in distal femora, and donor's gender and age. The size of the defect is also reflected by dividing defect volume (DV) with epiphyseal volume (EPV), which is considered from the distal end to the beginning of the intramedullary canal.

Samples	Defect Size		Defect Location				Donor	
Number	DV/EPV (%)	Volume (cc)	Anatomical Side	Contralateral Condyle Involvement	Epiphysis	Metaphysis	Gender	Age
Sample 1	17%	29.8	Medial	No	*		Male	64
Sample 2	19%	24.1	Medial	No	*		Male	39
Sample 3	26%	50.2	Medial	No	*	*	Male	34
Sample 4	31%	40.2	Lateral	Slightly	*	*	Female	46
Sample 5	32%	38.1	Lateral	Slightly	*	*	Male	48
Sample 6	36%	65	Medial	To some extent	*	*	Female	41
Sample 7	37%	59.7	Medial	To some extent	*	*	Female	32

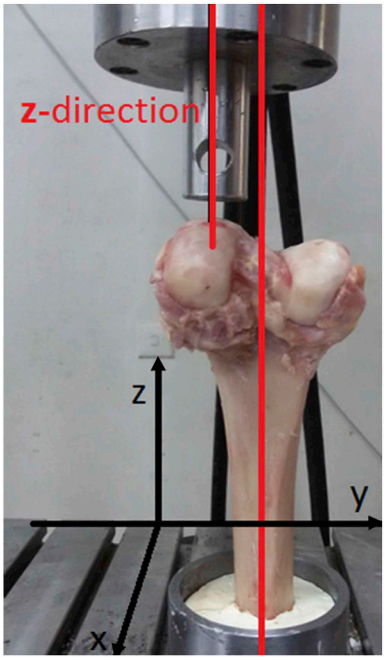

Fig. 2. The specimen was positioned in the test machine in such a way that the bone diaphysis was aligned in the z-direction, parallel to the machine cylinder that applied the compressive load on the medial condyle.

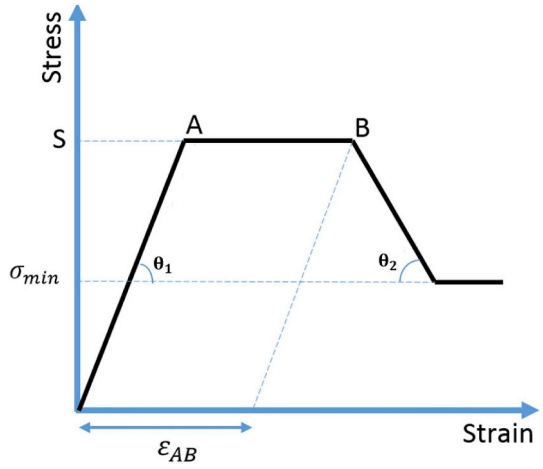

Fig. 3. Quad-linear stress-strain behavior was used for distal femoral bone. The model is described by an elastic phase with an elastic modulus of $E = \tan\theta_1$ until it reaches the yield stress (S), it is then followed by a perfect plastic phase with a plastic strain of ε_{AB} and a softening phase with a plastic modulus of $Ep = \tan\theta_2$ until it reaches minimum stress, σ_{min}, and finally a second perfect plastic phase.

indicator of fracture risk, was considered as the primary point in evaluating the response of the model [40]. The femoral shaft was potted in bone cement fixing it in all directions. Mechanical tests mimicked a single-leg-stance configuration with the load applied on the medial condyle. A preload of 100 N was applied on each specimen to first get a stabilized reading of force and displacement before the main load application, which was then applied with a quasi-static rate of 1 mm/min via a 20 mm-diameter actuator until macroscopic failure occurred in the femur. Data corresponding to the reaction force and displacement of the machine actuator was recorded, and the resulting force-displacement curve was obtained. Maximum force in the curve was defined as the experimentally measured fracture load (F_{Exp}). The specimen preparation, QCT scanning, and mechanical tests were done in one day to decrease the risk of bone damage and change in material properties due to refreezing. The specimen was defrosted only once to room temperature.

2.2. Computational part

Three-dimensional models of all femora specimens were created, meshed and assigned material properties by importing the QCT images into modeling software (Simpleware, Scan IP, and Scan FE V. 3.1). Using the tools and filters provided in the software, bone (including both cancellous and compact bones) and cement were segmented. Voxel meshing was selected for the whole model, in which each pixel from the 2-D images was converted into an 8-node brick element (Fig. 4A). In order to reduce computation time and make use of previously published relationships [41] for bone material properties (Table 2), the original DICOM[1] images with a resolution of 512*512 pixels and a pixel size of 0.5 mm were resampled to produce images with a resolution of 128*128 pixels with a pixel size of 2 mm. Hence, the number of elements was reduced to 25% of their initial value. The final 14 models consisted of 26563–44442 linear hexahedral elements with a length of 2 mm and 31222 to 56237 nodes depending on the specimen size.

The PMMA bone cement was assumed to have homogenous material properties. A symmetrical bi-linear, elastic-plastic constitutive law for cement material was assumed to have a Young's modulus, yield stress, and Poisson's ratio of: 2 GPa [24], 40 MPa [42] and 0.23 [24], respectively. In order to derive heterogeneous mechanical properties of bone from CT data, two sets of relationships were needed: one to convert HUs to ρ_{ash}, and the second to convert ash densities to bone material properties. Linear calibration coefficients, needed to calibrate ρ_{ash} from HUs were derived using the relationship specific to the calibration phantom used [36]. Compact and cancellous bone were differentiated based on the calculated ρ_{ash}. Poisson's ratio was considered to be constant and equal to 0.4 for both spongy and compact bone [43,44]. The constitutive law considered for bone in this study included a quad-linear elastic and post yield behavior as introduced by Keyak et al. [33]. The

[1] Digital Imaging and Communications in Medicine.

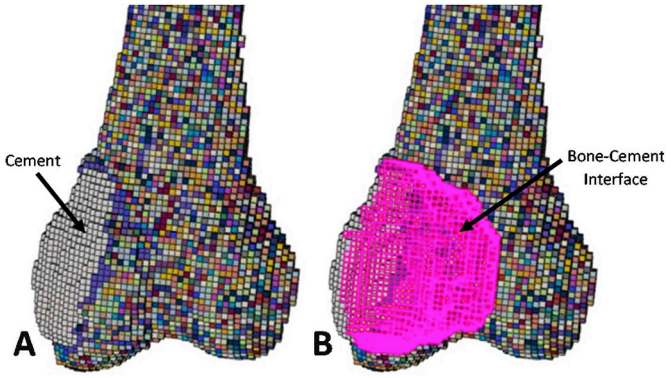

Fig. 4. (A) Voxel-based finite element model of a bone reconstructed with bone cement, and (B) Surface to surface contact made at the bone-cement interface between the two surfaces of hexahedral elements connected 1. To the bone and 2. To the cement is shown in pink.

Table 2
Material properties' relationships based on local bone ash density [33].

Relationship	Bone type	
	Cancellous	Compact
$E\ (MPa) = 14900\rho_{ash}^{1.86}$	×	×
$S\ (MPa) = 102\rho_{ash}^{1.80}$	×	×
$\varepsilon_{AB} = 0.00189 + 0.0241\rho_{ash}^{*}$	×	
$\varepsilon_{AB} = 0.0184 - 0.0100\rho_{ash}^{*}$		×
$E_p\ (MPa) = -2080\rho_{ash}^{1.45*}$	×	
$E_p\ (MPa) = -1000^{*}$		×
$\sigma_{min}\ (MPa) = 43.1\rho_{ash}^{1.81}$	×	×

*To account for the difference between the model element size and the specimen size for which the formula were obtained, these relationships must be modified before inclusion in FE models according to following equations [62]: for cancellous bone, $\varepsilon'_{AB} = \varepsilon_{AB} \times \frac{15}{2}$, $E'_p = \frac{2EE_p}{[15E-(15-2)E_p]}$, and for compact bone.$\varepsilon'_{AB} = \varepsilon_{AB} \times \frac{5}{2}$,$E'_p = \frac{2EE_p}{[5E-(5-2)E_p]}$

bone was assumed to behave as a linear elastic material until its yield point. Post failure behavior for each element was defined with an initial perfect plastic phase, followed by a softening phase until a minimum stress was reached, and then a perfectly plastic phase again as shown in Fig. 3. The relationships for deriving material properties based on ash density are shown in Table 2. The relationships for ε_{AB} and E_p found by Keyak et al. [33] were experimentally derived using strain measurement across cortical and trabecular specimens with the length of 5 and 15 mm, respectively, and the length of each cubic element used in this work was 2 mm. These relationships need to be modified because previous experiments have shown that specimen failure occurs locally in regions smaller than the size of bony specimens tested; hence, the plastic strain and modulus should be calculated for the locally yielded region not the whole specimen [41]. The modified relationships are given in the footnote of Table 2. Since the plastic phase of bone mechanical behavior was being considered, the engineering stress and strains calculated using the formulas described in Table 2 were converted to true stresses and strains before being imported into the FE models.

Boundary conditions mimicking in-vitro mechanical tests were applied to the models, so the femur shaft, equal to the length fixed in the experiment, was restricted in all directions. Surface to surface contact, with small sliding and cohesive behavior, was considered for the contact between bone and cement. For this purpose, two meshed based surfaces, made at the interface of hexahedral elements on the surfaces between the bone and cement (one on the bone and the other one on the cement), were defined. In Fig. 4B, the contact at the interface of bone and cement made by the surfaces of hexahedral elements is shown. The properties assigned for the interface assumed an intermediate interdigitation of the surrounding trabecular bone with the cement. Damage modeling was considered, using a traction-separation law, to investigate the debonding and damage initiation as well as damage propagation at the interface [45,46].

Nodes of the medial condyle, which were in contact with the 20 mm diameter actuator in the mechanical tests, were identified and an elastic modulus of 20 GPa and yield strength of 200 MPa were assigned to the elements containing those nodes to prevent severe distortion while being loaded as suggested in previous studies [33,36]. A displacement equal to 1 cm was applied to those nodes in the form of compression in the direction of the femoral shaft. This displacement was enough to result in the peak value of the force-displacement graph. Sum of the reaction forces at the displaced nodes versus their average displacement was calculated, then the force-displacement curve was plotted, and the maximum force on the force-displacement curve was defined as FE predicted fracture load (F_{FE}). FE simulations were solved in a static step with ABAQUS (v. 6.13–4, Dassault Systèmes) in conjunction with assuming material non-linearity and large deformations. The FE results were analyzed using the distortion failure energy theory, which is a validated theory for bone failure [47]. Study design from specimen preparation to FE analysis can be seen in Fig. 5.

The FE models were divided into two groups to evaluate and validate: the tuning group (TG) including five femora, and the evaluation group (EG) including nine femora. The femora were randomly divided between the two groups. Three intact femora and two femora with defects were included in the TG and the remaining four intact and five femora with simulated curettage and cementation were included in the EG. A code was written in MATLAB (v. 2009a) to reduce the values of E, S, and E_P by one percent per cycle and to create a new input file for models of the TG. Therefore, the aforementioned material properties of all five models of the TG were simultaneously reduced by the same percentage. This reduction in material properties was made to account for various issues causing systemic errors in the models, such as ignoring anisotropy, as suggested by Refs. [33,48]. Since the formulas of material properties were obtained for the longitudinal direction of bone (see Table 2), by considering isotropic properties for bone, properties in transverse directions are overestimated [49]. Other material properties in Table 2 retained their initial values because previous studies have not shown any other significant direction dependency [33]. Each input file was imported into ABAQUS to calculate the fracture load through FE analysis. Reduction in the aforementioned material properties (i.e., E, S, and E_P) continued until the following two criteria were met: 1) the difference between fracture load obtained from FE analysis (F_{FE}) and the experiment (F_{Exp}) was not different from zero by applying a paired *t*-test; and 2) linear regression analysis gave a relationship between F_{FE} and F_{Exp} with a slope not different from 1. The final set of material properties, which met the two criteria stated above, were then applied to the models of EG as an independent data set. In order to evaluate the accuracy and precision of the predicted strength, a paired *t*-test was then employed to determine if the difference between the strength calculated by FE analysis and the experimental results from the EG were significant (a P value less than 0.05 was considered statistically significant). The relationship between fracture load obtained from FE analysis and experimental data from the EG was also computed using linear regression analysis. In addition, the 95% confidence intervals of the difference and linear equation between F_{FE} and F_{Exp} for TG and EG were calculated and compared.

After the FE models were validated, they were extended to investigate the mechanics of the BCI by analyzing the damage, contact status, and the onset of crack at the BCI, which were impossible to investigate in the laboratory. XFEM was used to investigate crack initiation and growth in the bone-cement interface. The enriched region

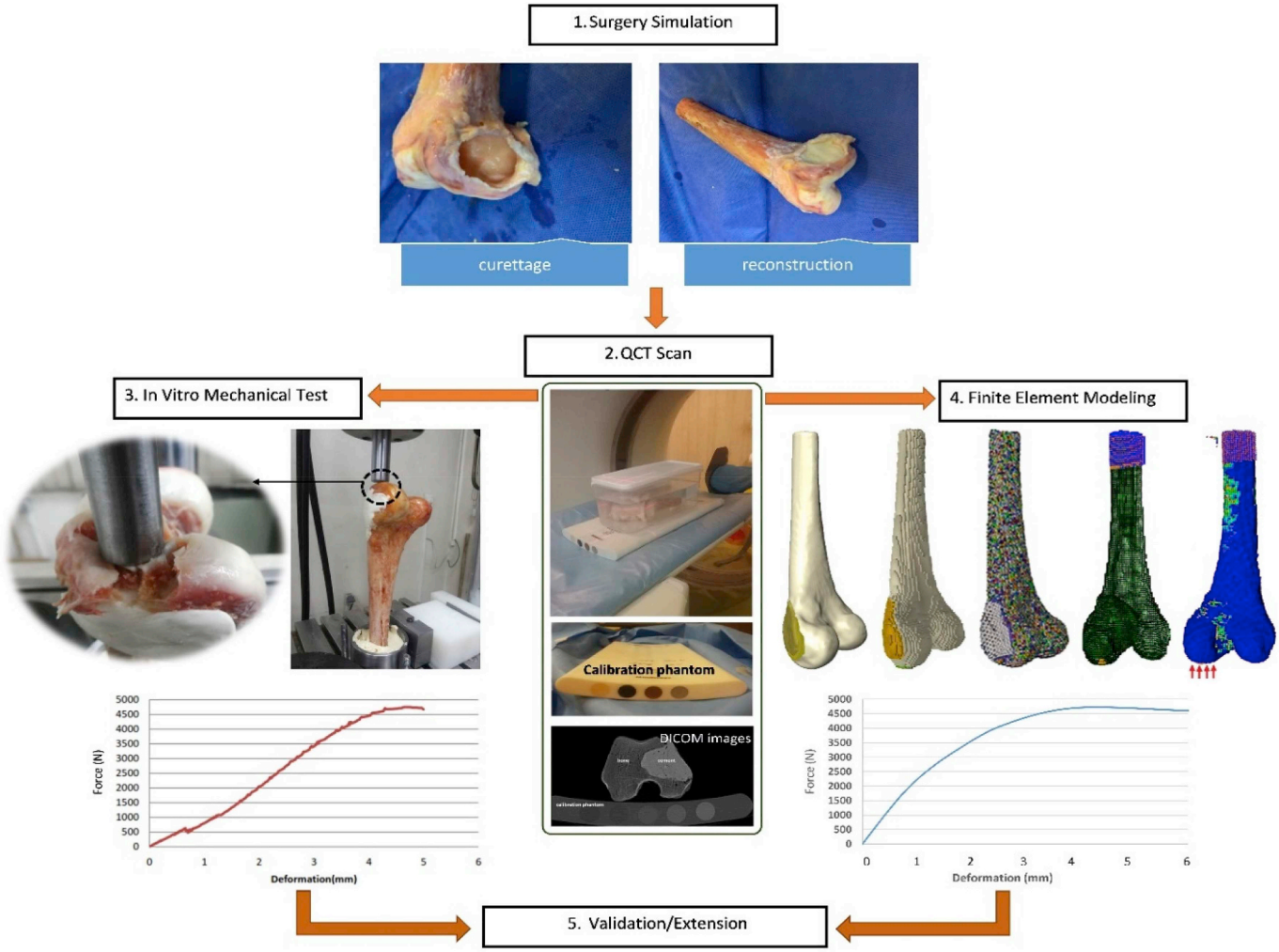

Fig. 5. The five steps involved in this study were: 1. Surgery simulation by creating a defect to mimic tumor curettage and defect infilling with bone cement to simulate reconstruction, 2. QCT scanning process, 3. In-vitro mechanical test and resultant force-deformation curve, 4. Finite element modeling, loading and boundary conditions and resultant force-deformation curve from FE analysis, and 5. Validation of FE models with in-vitro tests' results, and lastly the extension of the FE models.

consisted of a thin layer with the thickness of one to two elements between bone and cement. This was considered the crack domain and accounted for the penetration region of cement into bone. The crack analysis was based on the traction-separation cohesive behavior approach. Elastic and damage properties for elements belonging to the crack domain were defined to describe initial tract and separation behavior, respectively. The elastic behavior was written in terms of an elastic constitutive matrix which relates the normal and shear stresses to the normal and shear separations of a cracked element [50]. The nominal traction stress vector, t, consists of the following components: t_n, t_s, and t_t, which represent the normal and the two shear tractions, respectively. The corresponding separations are denoted by δ_n, δ_s, and δ_t. The elastic behavior is written as [50]:

$$t = \begin{bmatrix} t_n \\ t_s \\ t_t \end{bmatrix} = \begin{bmatrix} K_{nn} & 0 & 0 \\ 0 & K_{ss} & 0 \\ 0 & 0 & K_{tt} \end{bmatrix} \begin{bmatrix} \delta_n \\ \delta_s \\ \delta_t \end{bmatrix} = K\delta \tag{1}$$

K_{nn}, K_{ss}, and K_{tt} are elastic stiffness components. Damage properties for enriched elements consist of the following features: a damage initiation criterion and a damage evolution law; the damage initiation was set by the critical maximum nominal stresses. We used maximum nominal stress criterion in ABAQUS which assumes that damage begins when the maximum nominal stress ratio as defined in Eq. (2), at the center of the enriched element reaches a critical value ($f = 1$):

$$f = MAX\left\{\frac{\langle t_n \rangle}{N_{max}}, \frac{t_t}{T_{max}}, \frac{t_s}{S_{max}}\right\} \tag{2}$$

N_{max}, T_{max}, and S_{max} represent the peak values of the nominal stresses in normal and two shear directions, respectively. Damage initiation occurs under tensile or shear stresses, and damage evolution was defined by a power-law mixed mode behavior based on energy dissipation. The area under the traction-separation curve was defined as the fracture energy due to damage in the normal and two shear modes. The values considered for the properties of XFEM enriched elements were based on an experimental study [45] and were previously used in a FE study [51]. These values are shown in Table 3.

Table 3
Maximum nominal stress (t) in the linear region, stiffness (K), and fracture energy (G) for normal and two shear directions considered for elements in the enriched region [51].

Stress Direction	t (MPa)	K (MPa/mm)	G (N/mm)
Normal (N)	1.47	21.08	0.479
Shear 1 (T)	2.1	25.75	1.06
Shear 2 (S)	2.1	25.75	1.06

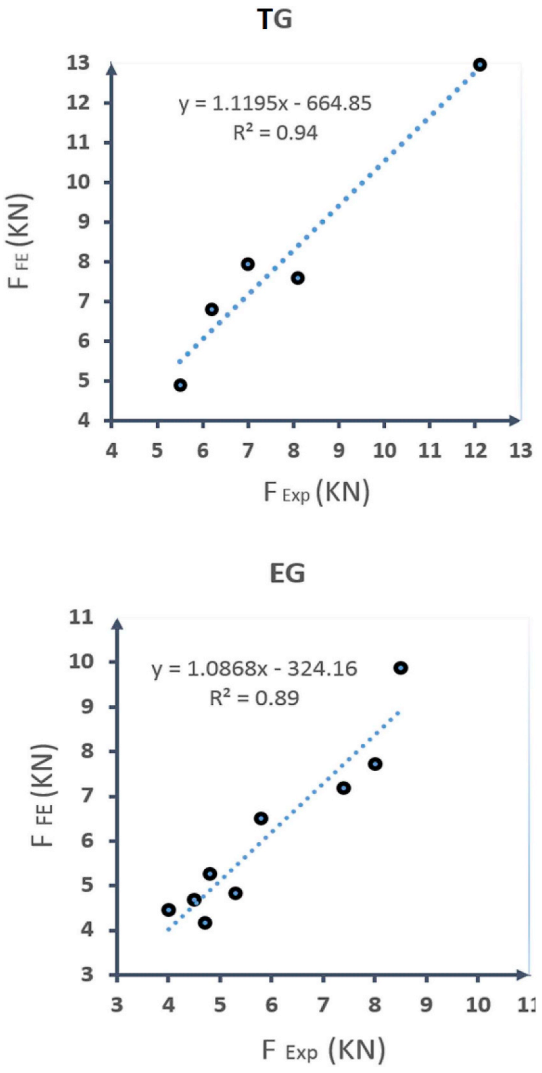

Fig. 6. Femoral ultimate strength found by FE analysis (F_{FE}) versus experimental (F_{Exp}) recorded for TG ($R^2 = 0.94$) and EG ($R^2 = 0.89$) using regression analysis.

3. Results

The MATLAB program and subsequent FE analysis were run for 17 cycles for each model to meet the following two conditions: 1) the error of F_{FE} - F_{Exp} not different from zero using a paired *t*-test, and 2) a 1:1 relationship between F_{FE} and F_{Exp} using linear regression analysis. Consequently, the elastic modulus, yield strength, and plastic modulus values were eventually reduced by 17% to produce data for the TG that resulted in an accurate computation of distal femoral strength, i.e., agreement with in-vitro tests results ($r^2 = 0.94$, $P \leq 0.05$). Then, the 17% reduced material properties were assigned to the EG models, as an independent data set, to evaluate the accuracy and precision of the predicted material properties. Comparison between the EG's F_{FE} and F_{Exp} yielded a coefficient of determination of 0.89, considering $P \leq 0.05$. Regression analysis showed a good linear relationship between F_{FE} and F_{Exp} for TG and EG with a slope not different from 1, as shown in Fig. 6. Results of the paired t-tests for both groups did not show a significant difference between the predicted FE and the experimentally recorded fracture loads ($p = 0.474$ for TG and $p = 0.396$ for EG). Statistical analysis was completed with SPSS software for windows, version 16 (SPSS Inc., Chicago, USA), and the outcomes are shown in Table 4. Precision of the predicted fracture load by FE analyses was described by a 95% confidence interval of the difference between F_{FE} and F_{Exp}. The upper limit of 95% confidence interval of the difference obtained from paired t-tests for TG and EG was 1197 N and 668 N, respectively.

Results of analyzing mechanics of the BCI including contact status, damage, and crack initiation for two models are shown in Fig. 7. Analysis of contact between bone and cement revealed larger sites for cement debonding from bone at the medial and interior walls of the interface for all models. Contact surface status after the load is applied for the lateral and medial defects of a left femur, for instance, are shown in Fig. 7B. The color of the interface is red if there is no contact separation, blue for complete separation, and green if the two faces of the interface are slipping on each other. The contact opening at the interior and medial sites of the interface can be seen in Fig. 7B, whereas the proximal and distal walls as well as small regions in the posterior and anterior walls, are still in contact after the load is applied for a bone model with a medial defect. As can be seen in Fig. 7B, sliding or closed contact regions were found on the distal and proximal walls of the interface for the medially located defects, while the anterior and posterior walls of the defect were still in contact for the laterally placed defects. Damage criterion was defined based on the maximum nominal stress (Eq. (2)), i.e., stress at the BCI normalized to critical stress for damage initiation, defined by the CSMAXSCRT variable [46]. This variable indicates if the maximum contact stress has been satisfied. In Fig. 7C, since the CSMAXCRT value is a parameter which denotes the damage propagation up to failure at the BCI, the proximal end of the cortical window, regardless of the site of the defect, can be deemed as the most critical site from where damage initiates and propagates. Small cracks initiation in the proximal end of the cortical window, which grew into the interior side of the interface, were predicted by the XFEM analysis (Fig. 7D). In addition, cement debonding from bone was observed at the interior wall of the interface (Fig. 7D).

4. Discussion

Cement augmentation following benign bone tumor surgery is the most common procedure for strengthening the affected bone with the aim of reducing the risk of post-operative fracture in patients with large defects. However, there is no firm biomechanical data to identify patients at high risk of fracture or to suggest the most suitable device for augmentation. Accurate assessment of bone strength following surgery, as a key determinant of fracture risk, would allow patients at high risk of fracture to be identified and inhibitory actions to be taken. Selection of a suitable fixation device(s) for cement augmentation requires a deep understanding of the mechanics of the BCI as well as a good estimation of bone strength. The proposed non-linear, QCT-based FEM can reasonably predict distal femoral strength; the accuracy and precision of the FE models were evaluated using statistical tests, which resulted in a good correlation between the FE models and the corresponding in-vitro experiments. In addition, critical sites where reconstruction failure may occur were predicted by taking into account the mechanics of the BCI, including three factors: 1) maximum stress and damage; 2) analysis of contact; and 3) crack initiation at the interface. The proximal end of the cortical window and the interior wall of the BCI were thus found to be the most critical sites of reconstruction failure.

Even though strong correlation was found between bone strength predicted by FE analyses and those found experimentally (Fig. 6), the accuracy and precision of the models can be improved by overcoming some of the existing limitations of this study. It is speculated that the main cause of the wide range of the 95% confidence interval for the slope of the predicted linear equation between F_{FE} and F_{Exp} (see Table 4) is due to the small number of specimens evaluated, particularly in the TG with only five femora. Although increasing the number of specimens may increase the precision of the results, the ethical concerns as well as the high cost and time-consuming nature of in-vitro experiments can be a major issue. Also, one of the main justifications for creating sophisticated FE models is that once they are validated they can replace in-vitro experiments for investigating the behavior of bone

Table 4
Relationship between F_{FE} and F_{Exp} presented using statistical tests.

		Linear regression equations	95% Confidence Interval (CI) for the slope of equations		95% Confidence Interval (CI) of $F_{FE\_}F_{Exp}$		R^2	Sig. (2-tailed)
Group	Pairs		Lower	Upper	Lower	Upper		
TG	$F_{FE\_}F_{Exp}$	$F_{FE} = 1.12\ F_{Exp} - 664.85$	0.637	1.602	−667	1197	0.94	0.474
EG	$F_{FE\_}F_{Exp}$	$F_{FE} = 1.08\ F_{Exp} - 324.16$	0.759	1.415	−293	668	0.89	0.396

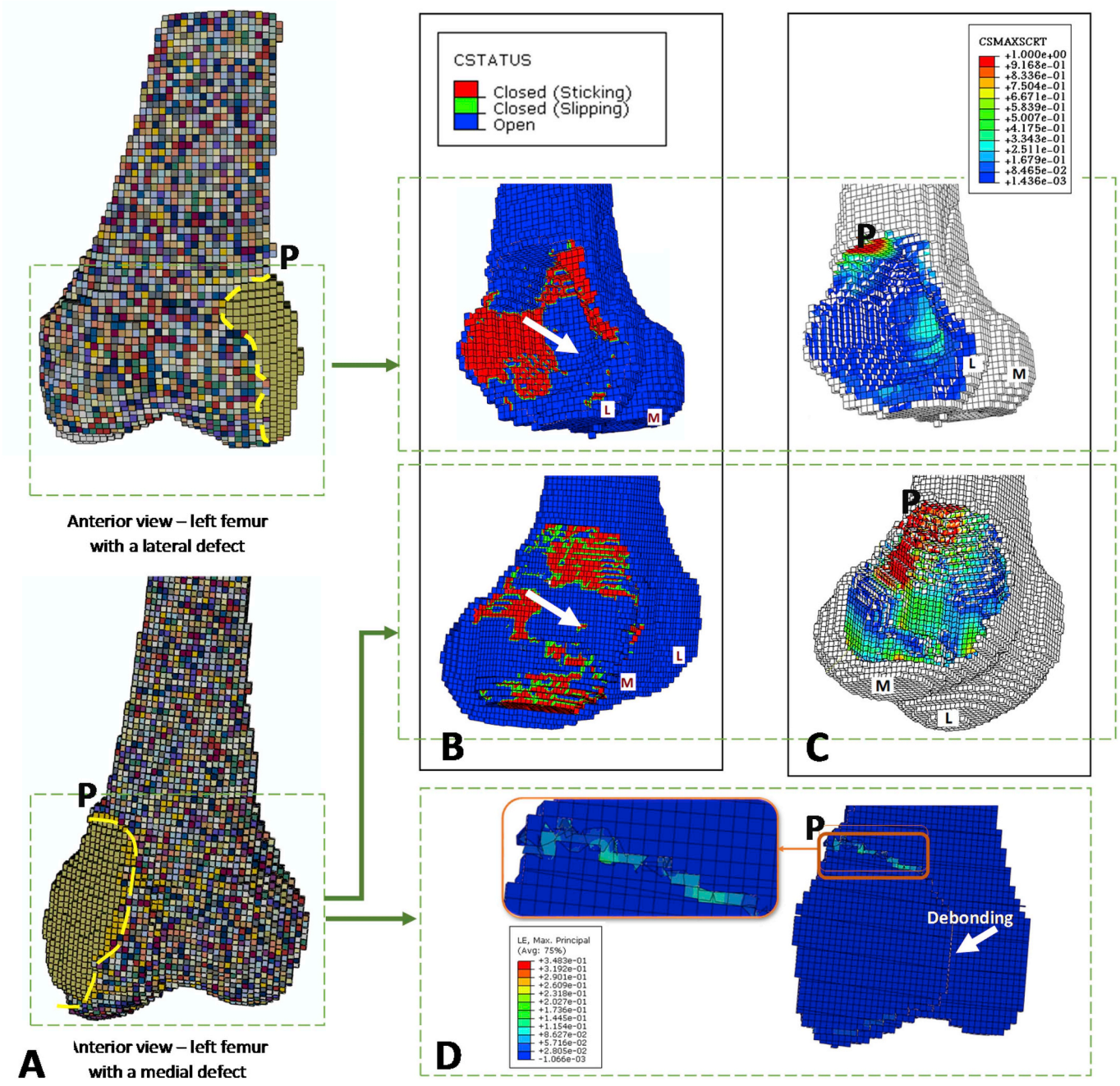

Fig. 7. FE analyses results associated with the mechanics of the BCI: (A) Anterior view of two femora with a laterally (top), and a medially (bottom) located defect, cortical window is indicated by dotted yellow lines; (B) Contact status, CSTATUS contour, shows a larger cement debonding area at the interior wall of the interface (L and M stand for lateral and medial, respectively); (C) Damage analysis, CSMAXSCRT contour, shows damage initiation at the proximal end of the cortical window, P; and (D) Cracks at the proximal end of the interface, P, which propagate into the interior and medial walls, are shown. The logarithmic strain, LE, shows maximum values at the site of the cracks. Cement debonding from the bone at the interior wall of the interface, indicated by white arrows, is apparent.

under desired loading and boundary conditions. Therefore, the validation procedure should be implemented with a small number of experiments to be cost-effective and meaningful [35]. Another limitation connected with FE modeling is the assumption of isotropic material properties as well as considering equal strength in tension and compression for cortical and cancellous bones. It is a well-known fact that cortical bone is transversely isotropic [52], and cancellous bone is orthotropic [53], and both show different behavior under tension and compression. Although, anisotropic properties could be theoretically obtained from isotropic properties of bone, nonetheless, relationships for direction dependence of material properties directly from CT scan data was not available [33]. Even with further development in CT scanning, assuming one could collect anisotropic properties of bone which take into account the differences in tensile and compression, the challenge of considering anisotropy in FEM remains due to lack of validated failure theories for multiaxial stress-strain states for bone [33]. The relationships in Table 2 were originally derived for the superior-inferior direction of bone [43], i.e., longitudinal direction, in which bone has the greatest strength, but were assigned to other directions in this work due to the simplifying assumption of bone isotropy. However, in order to somehow compensate for this simplification and compromise with real, anisotropic behavior of bone [33,43], the values of elastic modulus, yield stress and plastic modulus (which are direction dependent) were reduced using the tuning process, which ultimately resulted in a good correlation between F_{FE} and F_{Exp} (see Table 4). Although anisotropy is an important source of systematic error, there are many other sources of errors, e.g., converting CT scan data to density and elastic modulus; modeling the boundary conditions; meshing or assigning material properties, as well as other contributing factors. Therefore, it should be kept in mind that the tuning approach accounted for all systematic sources of error simultaneously, and is not just for disregarding anisotropy in the model. The tuning process's goal in this study is to correct all possible issues in the FE analysis that may lead to a systematic error in the modeling approach. The use of the tuning process to address systematic errors makes simulation results compatible and close to those of experimental outcomes. For example, tuning process can address the dissimilar outcomes resulting from differing element sizes, or the different fracture loads caused due to mismatched in boundary conditions between in-silico model and in-vitro experiment. The presented method suffers from limitations due to the use of the tuning process. Although it is known that the method presented in this study is correcting for systematic errors, however since it is not a mechanistic approach, the specific errors and their order of magnitude compared with other sources of errors is not known. It remains unclear what exactly the tuning process takes into account, and how much of the tuning can be attributed to a particular source of the systematic error. Disregarding articular cartilage and the effect of its deformation when the compression load was applied on the bone in the FE models and the consequent lack of comparison of stiffness and strain energy between in-silico and in-vitro results is another limitation of this work. Segmentation and differentiation of the exact geometry of the articular cartilage from QCT images was not possible due to its similar attenuation with the surrounding fluid. Since articular cartilage was not modeled and was excluded from the FE models, the deformation of the bone predicted by FEA was different from those recorded in the experiments, i.e., the deformation at each specific force was higher in the experiments compared to the deformation predicted by FEA. However, it is interesting to note that no significant difference was observed in the maximum loads measured by in-silico models and in-vitro tests, which makes sense considering the almost negligible contribution of articular cartilage in the maximum load carrying capacity of the construct. Therefore, it was not logical to compare and validate the FE models by finding stiffness or strain energy. Additionally, it was not possible to accurately predict both the fracture load and strain unless an anisotropic FE model was used or an anisotropic failure theory, which is currently unknown, could be employed. Stiffness and strain energy depend on the strain as well, so it has the same problem. Thus, even though the fracture load predicted by the presented method is correct and reliable, it does not indicate that the stress or strain values are necessarily accurate. This is due to our use of the isotropic properties of bone, which prevented us from obtaining accurate stresses or strains by limiting us to use just one modulus for all directions.

An essential step in deriving material properties from CT data, which can have considerable effect on the accuracy of FE models, is the selection of the proper relationships for converting bone density values measured by QCT to bone material properties from the variety of relationships that have been previously reported [33–36]. Since the relationship between density and modulus are site-specific [54], the equations for the human distal femoral trabecular and cortical bone found by Kayak et al. [33] were used in this study. Since these relationships give a wide range for moduli and strength (E = 0.6–23 GPa and S = 5–160 MPa) [33], they can be used for both cancellous and compact bone. The accuracy of the FE models, evaluated by paired t-tests, showed the robustness of the presented non-linear and heterogeneous QCT-based FE models in predicting bone strength and were found to be in agreement with in-vitro experiments on the corresponding cadaveric specimens (see Table 4). The value of the upper limit of 95% confidence interval of F_{FE} - F_{Exp}, as a measure of the FE models precision, for both groups (Table 4) was in the range of previously reported data, and is acceptable for clinical use [33]. Hence, the accuracy and precision of the FE models of bone following a simulated tumor surgery in the distal femur were validated by in-vitro tests. Thus, the models could be extended to investigate other important aspects of the problem, such as the mechanics of the BCI, which are difficult or even impossible to experimentally or clinically study.

Another important, but inevitable limitation of this work was the use of cadaveric specimens to conduct mechanical loading tests to validate the FE models, with the ultimate goal of investigating an in-vivo situation. It should be noted that, however, deriving accurate material properties of bone from QCT-scans of patients is accompanied by challenges due to the artifacts caused by surrounding tissues. Since computing bone strength on live subjects is not practical, increased uncertainty in predicting bone strength and mechanics of the BCI should be kept in mind when using results of an in-silico model validated by in-vitro experiments to study in-vivo cases.

One of the unique aspects of this work was the investigation made on the mechanics of the BCI, with the scope of finding vulnerable regions where fracture is more likely to happen by utilizing XFEM to predict cracks initiation and growth as well as contact analysis at the BCI, which have not been considered in previous studies to date [12,24]. Predefining the path of crack propagation and remeshing, unlike conventional FEM, were not needed in the XFEM used. This unique advantage of XFEM allowed the prediction of crack propagation at the BCI. One of the limitations of the XFEM approach is its convergence problem and the elastic property of the enriched region [50]. The convergence difficulty was addressed by modifying the solution control parameters. It is well known that assuming bone as a linear elastic material is just a simplification, but one has to compromise between modeling actual properties of bone and determining the crack path using XFEM. Considering plastic and post-failure properties were essential in predicting bone strength. Hence, in this work the XFEM domain, including elements with just elastic properties, was limited to a thin layer at the interface of bone-cement. Cracks were anticipated at the BCI, and thus the onset of cracks at the interface could be investigated, but the actual crack growth path in the whole bone model was not traceable. The crack growth and direction of propagation in the surrounding bone could be determined if the enriched region also included the neighboring bone, which was not the case in this study.

Analysis of contact at the BCI showed that larger debonding areas would occur in the medial and interior walls of the interface (see Fig. 7B). Cement debonding may be the main cause of reconstruction failure requiring cement augmentation. Therefore, in order to

strengthen the reconstruction, it is reasonable to advise that a strong cement augmentation should cross the interior wall of the interface. Based on XFEM analyses at the BCI, the proximal end of the cortical window was found to be the most vulnerable site where cracks can initiate and may result in a fracture (see Fig. 7C and D). Thus, this site must also be reinforced by augmenting the cement with internal fixation devices to reduce the likelihood of fracture. Intramedullary pins, screws, and plates, common configurations shown in Fig. 1, are used for cement augmentation in distal femoral defects caused by tumor removal [24,55–57]. Bearing in mind the placement of assistive devices and critical sites at the interface of bone and cement found in this study (see Fig. 7), screws may have a mechanical advantage over intramedullary pins as a result of reinforcing one of the critical sites, the medio-interior wall of the interface as (see Fig. 1A). A plate seems to better to strengthen the bone, compared to intramedullary pins and screws, because it bridges the most critical sites of fracture, i.e., the proximal end of the cortical window (see Fig. 1C); moreover, its screws cross the interior and medial parts of the BCI where cement debonding may occur (see Fig. 1C). In addition, considering the configuration of pins (Fig. 1B) and two critical sites at the interface based on this study's outcomes (see Fig. 7), it is speculated that augmenting the cement with intramedullary pins cannot be very advantageous as pins can neither support the debonding nor the crack initiation areas. A comparative study on the performance of intramedullary Steinmann pins and crossed screws engaging the opposite cortex for cement augmentation in distal femoral defects has shown higher bone strength when augmented with screws crossing the cement debonding sites [37]. In addition, there are several experimental studies on human cadaveric bones showing no biomechanical advantages in using intramedullary Steinmann pins for augmenting cement [55,58,59]. Moreover, some previous *in-vitro* studies related to the best fixation devices to augment cement for distal femoral and proximal tibialis defects support the findings of this study by demonstrating the superiority of plates, compared to other internal fixation devices [57,60]. However, it should be noted that some other factors, such as the load transfer when an implant is used, or the bone related factors, such as its size or density, may also contribute to the results obtained in the aforementioned in-vitro studies. In order to find the best fixation device for cement augmentation, besides making experimental investigations, the FE models should also contain those implants beside bone, to make the analyses more accurate and trustable. Moreover, the contact properties between the implant and bone, as well as cement and bone should be considered.

5. Conclusions

This study established a non-linear, QCT-based FEM for estimating bone strength following a benign bone tumor simulated surgery, with the ultimate goal of developing current clinical criteria in identifying patients at high risk of postoperative fractures, and thus achieve better surgical outcomes. The validated FE models can be extended to investigate the effect of defect size on the risk of bone fracture so that a quantitative criterion can be proposed for *large* defects which require cement augmentation. It was thought that understanding the mechanics of a BCI, for instance by finding vulnerable locations of failure and fracture initiation, could provide the identification of some causes of reconstruction failure, and thus provide the initiative for the creation of safer cement augmentation tools. It is hoped that information gained in this kind of research will shed light on selecting safer surgical techniques as well as aid in choosing or designing better fixation devices which will ultimately reduce the risk of postoperative fracture in bone cancer patients.

Declarations of interest for all authors

None.

Formatting of funding sources

This research did not receive any specific grant from funding agencies in the public, commercial, or not-for-profit sectors.

Conflicts of interest

Azadeh Ghouchani: None Declared.
Gholamreza Rouhi: None Declared.
Mohammad H. Ebrahimzadeh: None Declared.

Acknowledgments

We thank Amirkabir University of Technology, Iran, for supporting this research. We sincerely thank Professor. Keyak for her valuable comments regarding the method used. We would also like to thank Dr. Akhlaghpour for his support in taking the QCT scans (Noor Clinic). The valuable help of Dr. E. Vahedi and Dr. M. Salehi, in mimicking tumor surgeries and interpreting the statistical tests results, respectively, is greatly appreciated.

References

[1] M. Werner, Giant cell tumour of bone: morphological, biological and histogenetical aspects, Int. Orthop. 30 (6) (2006) 484–489.
[2] A.H. Kivioja, C. Blomqvist, K. Hietaniemi, C. Trovik, A. Walloe, H.C. Bauer, P.H. Jorgensen, P. Bergh, G. Follerås, Cement is recommended in intralesional surgery of giant cell tumors: a Scandinavian Sarcoma Group study of 294 patients followed for a median time of 5 years, Acta Orthop. 79 (1) (2008) 86–93.
[3] R.C. Marcove, L.D. Weis, M.R. Vaghaiwalla, R. Pearson, Cryosurgery in the treatment of giant cell tumors of bone, Clin. Orthop. Relat. Res. 134 (1978) 275–289.
[4] A. Ghouchani, G. Rouhi, The great need of a biomechanical-based approach for surgical methods of giant cell tumor: a critical review, J. Med. Biol. Eng. 37 (4) (2017) 454–467.
[5] N. Fraquet, G. Faizon, P. Rosset, J.-M. Phillipeau, D. Waast, F. Gouin, Long bones giant cells tumors: treatment by curretage and cavity filling cementation, Orthop. Traumatol. Surg. Res. 95 (6) (2009) 402–406.
[6] O. Ofluoglu, Aggressive treatment of giant cell tumour with multiple local adjuvants, Acta Orthop. Belg. 74 (6) (2008) 831.
[7] A. Puri, M. Agarwal, Treatment of giant cell tumor of bone: current concepts, Indian J. Orthop. 41 (2) (2007) 101–108.
[8] A. Ghouchani, M.H. Ebrahimzadeh, G. Rouhi, The most appropriate reconstruction method following giant cell tumor curettage: a biomechanical approach, Arch. Bone Jt. Surg. 6 (2) (2018) 85.
[9] M. Hirn, U. de Silva, S. Sidharthan, R.J. Grimer, A. Abudu, R.M. Tillman, S.R. Carter, Bone defects following curettage do not necessarily need augmentation: a retrospective study of 146 patients, Acta Orthop. 80 (1) (2009) 4–8.
[10] T. Yanagawa, H. Watanabe, T. Shinozaki, K. Takagishi, Curettage of benign bone tumors without grafts gives sufficient bone strength: a case-series of 78 patients, Acta Orthop. 80 (1) (2009) 9–13.
[11] M.H. Taraz-Jamshidi, M. Gharadaghi, S.M. Mazloumi, M. Hallaj-Moghaddam, M.H. Ebrahimzadeh, Clinical outcome of en-block resection and reconstruction with nonvascularized fibular autograft for the treatment of giant cell tumor of distal radius, J. Res. Med. Sci. 19 (2) (2014) 117–121.
[12] H. Mosleh, G. Rouhi, A. Ghouchani, J. Nourisa, N. Bagheri, Prediction of the fracture risk of reconstructed bone with cement using QCT based structural rigidity and finite element analysis, Orthopaedic Research Society Annual Meeting San Diego, California, 2017.
[13] G. Rouhi, A. Vahdati, X. Li, L. Sudak, A three dimensional computer model to simulate spongy bone remodelling under overload using a semi-mechanistic bone remodelling theory, J. Mech. Med. Biol. 15 (04) (2015) 1550061.
[14] K. Haase, G. Rouhi, Prediction of stress shielding around an orthopedic screw: using stress and strain energy density as mechanical stimuli, Comput. Biol. Med. 43 (11) (2013) 1748–1757.
[15] A. Chitsazan, W. Herzog, G. Rouhi, M. Abbasi, Alteration of strain distribution in distal tibia after triple arthrodesis: experimental and finite element investigations, J. Med. Biol. Eng. (2017) 1–13.
[16] S. Samsami, S. Saberi, S. Sadighi, G. Rouhi, Comparison of three fixation methods for femoral neck fracture in Young adults: experimental and numerical investigations, J. Med. Biol. Eng. 35 (5) (2015) 566–579.
[17] R. Huiskes, R. Ruimerman, G.H. Van Lenthe, J.D. Janssen, Effects of mechanical forces on maintenance and adaptation of form in trabecular bone, Nature 405 (6787) (2000) 704.
[18] J. Nourisa, G. Rouhi, Biomechanical evaluation of intramedullary nail and bone plate for the fixation of distal metaphyseal fractures, J. Mech. Behav. Biomed. Mater. 56 (2016) 34–44.
[19] G. Rouhi, M. Tahani, B. Haghighi, W. Herzog, Prediction of stress shielding around orthopedic screws: time-dependent bone remodeling analysis using finite element approach, J. Med. Biol. Eng. 35 (4) (2015) 545–554.

[20] A. Vahdati, G. Rouhi, A model for mechanical adaptation of trabecular bone incorporating cellular accommodation and effects of microdamage and disuse, Mech. Res. Commun. 36 (3) (2009) 284–293.

[21] A. Araujo, L.M. Cook, C.C. Lynch, D. Basanta, An integrated computational model of the bone microenvironment in bone-metastatic prostate cancer, Cancer Res. 74 (9) (2014) 2391–2401.

[22] F. Eggermont, L. Derikx, N. Verdonschot, I. Van der Geest, M. De Jong, A. Snyers, Y. Van der Linden, E. Tanck, Can patient-specific finite element models better predict fractures in metastatic bone disease than experienced clinicians? Towards computational modelling in daily clinical practice, Bone Joint Res. 7 (6) (2018) 430–439.

[23] G. Salvatore, A. Berton, H. Giambini, M. Ciuffreda, P. Florio, U.G. Longo, V. Denaro, A. Thoreson, K.-N. An, Biomechanical effects of metastasis in the osteoporotic lumbar spine: a Finite Element Analysis, BMC Muscoskelet. Disord. 19 (1) (2018) 38.

[24] J. Li, F. Wodajo, M. Theiss, M. Kew, A. Jarmas, Computer simulation techniques in giant cell tumor curettage and defect reconstruction, Comput. Sci. Eng. 15 (2) (2013) 21–26.

[25] M. Jasty, W. Maloney, C. Bragdon, D. O'connor, T. Haire, W. Harris, The initiation of failure in cemented femoral components of hip arthroplasties, J. Bone Joint. Surg. Br. 73 (4) (1991) 551–558.

[26] T. Bousnane, S. Benbarek, A. Sahli, B. Serier, B.A.B. Bouiadjra, Damage of the bone-cement interface in finite element analyses of cemented orthopaedic implants, Period. Polytech. - Mech. Eng. 62 (2) (2018) 173–178.

[27] J.-Y. Wang, G. Tozzi, J. Chen, F. Contal, C. Lupton, J. Tong, Bone–cement interfacial behaviour under mixed mode loading conditions, J. Mech. Behav. Biomed. Mater. 3 (5) (2010) 392–398.

[28] T. Wada, M. Kaya, S. Nagoya, S. Kawaguchi, K. Isu, T. Yamashita, S. Yamawaki, S. Ishii, Complications associated with bone cementing for the treatment of giant cell tumors of bone, J. Orthop. Sci. 7 (2) (2002) 194–198.

[29] A.R. Khoei, Extended Finite Element Method: Theory and Applications, John Wiley & Sons, 2014.

[30] A. Idkaidek, I. Jasiuk, Cortical bone fracture analysis using XFEM–case study, Int. J. Numer. Methods Biomed . Eng. 33 (4) (2017) e2809.

[31] A.E. Vellwock, L. Vergani, F. Libonati, A multiscale XFEM approach to investigate the fracture behavior of bio-inspired composite materials, Compos. B Eng. 141 (2018) 258–264.

[32] A.A. Abdel-Wahab, A.R. Maligno, V.V. Silberschmidt, Micro-scale modelling of bovine cortical bone fracture: analysis of crack propagation and microstructure using X-FEM, Comput. Mater. Sci. 52 (1) (2012) 128–135.

[33] J. Keyak, T. Kaneko, J. Tehranzadeh, H. Skinner, Predicting proximal femoral strength using structural engineering models, Clin. Orthop. Relat. Res. 437 (2005) 219–228.

[34] K.K. Nishiyama, S. Gilchrist, P. Guy, P. Cripton, S.K. Boyd, Proximal femur bone strength estimated by a computationally fast finite element analysis in a sideways fall configuration, J. Biomech. 46 (7) (2013) 1231–1236.

[35] Finite element prediction and experimental verification of the failure pattern of proximal femur using quantitative computed tomography images, in: M. Mirzaei, S. Samiezadeh, A. Khodadadi, M.R. Ghazavi (Eds.), Proceedings of the International Conference on Biomechanics and Biomedical Engineering, Copenhagen, Denmark, 2012.

[36] M. Mirzaei, M. Keshavarzian, V. Naeini, Analysis of strength and failure pattern of human proximal femur using quantitative computed tomography (QCT)-based finite element method, Bone 64 (2014) 108–114.

[37] E. Schileo, F. Taddei, L. Cristofolini, M. Viceconti, Subject-specific finite element models implementing a maximum principal strain criterion are able to estimate failure risk and fracture location on human femurs tested in vitro, J. Biomech. 41 (2) (2008) 356–367.

[38] K. Motamedi, L.L. Seeger, Benign bone tumors, Radiol. Clin. 49 (6) (2011) 1115–1134.

[39] A. Sobti, P. Agrawal, S. Agarwala, M. Agarwal, Giant cell tumor of bone-an overview, Arch. Bone Jt. Surg. 4 (1) (2016) 2.

[40] Y. Lin, L. Ma, Y. Zhu, Z. Lin, Z. Yao, Y. Zhang, C. Mao, Assessment of fracture risk in proximal tibia with tumorous bone defects by a finite element method, Microsc. Res. Tech. 80 (2017) 975–984.

[41] J. Journal of Community Health NursingKeyak, I. Lee, D. Nath, H. Skinner, Postfailure compressive behavior of tibial trabecular bone in three anatomic directions, J. Biomed. Mater. Res. 31 (3) (1996) 373–378.

[42] Q.-H. Zhang, G. Tozzi, J. Tong, Micro-mechanical damage of trabecular bone–-cement interface under selected loading conditions: a finite element study, Comput. Methods Biomech. Biomed. Eng. 17 (3) (2014) 230–238.

[43] J. Keyak, H.B. Skinner, J.A. Fleming, Effect of force direction on femoral fracture load for two types of loading conditions, J. Orthop. Res. 19 (4) (2001) 539–544.

[44] L. Grassi, S.P. Väänänen, M. Ristinmaa, J.S. Jurvelin, H. Isaksson, How accurately can subject-specific finite element models predict strains and strength of human femora? Investigation using full-field measurements, J. Biomech. 49 (5) (2016) 802–806.

[45] K. Mann, D. Ayers, F. Werner, R. Nicoletta, M. Fortino, Tensile strength of the cement-bone interface depends on the amount of bone interdigitated with PMMA cement, J. Biomech. 30 (4) (1997) 339–346.

[46] Numerical modelling of adhesive connections including cohesive damage, in: C. Bedon, K. Machalická, M. Eliášová, M. Vokáč (Eds.), Challenging Glass Conference Proceedings, 2018.

[47] J. Keyak, S. Rossi, Prediction of femoral fracture load using finite element models: an examination of stress-and strain-based failure theories, J. Biomech. 33 (2) (2000) 209–214.

[48] J. Keyak, S. Sigurdsson, G. Karlsdottir, D. Oskarsdottir, A. Sigmarsdottir, J. Kornak, T. Harris, G. Sigurdsson, B. Jonsson, K. Siggeirsdottir, Effect of finite element model loading condition on fracture risk assessment in men and women: the AGES-Reykjavik study, Bone 57 (1) (2013) 18–29.

[49] T.M. Keaveny, E.F. Morgan, O.C. Yeh, Bone mechanics, in: K. Myer (Ed.), Standard Handbook of Biomedical Engineering and Design, McGrew Hill Professional, 2004, pp. 1–24.

[50] cited 2018 September 7, Modeling Discontinuities as an Enriched Feature Using the Extended Finite Element Method 2018, (2018) Abaqus 6.14 user's guide:[Available from: https://www.sharcnet.ca/Software/Abaqus/6.14.2/v6.14/books/usb/default.htm?startat=pt04ch10s07at36.html#usb-anl-aenrichment.

[51] T. Bousnane, S. Benbarek, A. Sahli, B. Serier, B.A.B. Bouiadjra, Damage of the bone-cement interface in finite element analyses of cemented orthopaedic implants, Period. Polytech. - Mech. Eng. 62 (2) (2018) 173–178.

[52] X.N. Dong, X.E. Guo, The dependence of transversely isotropic elasticity of human femoral cortical bone on porosity, J. Biomech. 37 (8) (2004) 1281–1287.

[53] M. Ciarelli, S. Goldstein, J. Kuhn, D. Cody, M. Brown, Evaluation of orthogonal mechanical properties and density of human trabecular bone from the major metaphyseal regions with materials testing and computed tomography, J. Orthop. Res. 9 (5) (1991) 674–682.

[54] R.W. Goulet, S.A. Goldstein, M.J. Ciarelli, J.L. Kuhn, M. Brown, L. Feldkamp, The relationship between the structural and orthogonal compressive properties of trabecular bone, J. Biomech. 27 (4) (1994) 375379–377389.

[55] P.J. Murray, T.A. Damron, J.K. Green, H.D. Morgan, F.W. Werner, Contained femoral defects: biomechanical analysis of pin augmentation in cement, Clin. Orthop. Relat. Res. 420 (2004) 251–256.

[56] P.C. Toy, J. France, R.L. Randall, M.D. Neel, R.I. Shorr, R.K. Heck, Reconstruction of noncontained distal femoral defects with polymethylmethacrylate and crossed-screw augmentation: a biomechanical study, J. Bone Jt. Surg. 88 (1) (2006) 171–178.

[57] A.D. Uglialoro, M. Maceroli, K.S. Beebe, J. Benevenia, F.R. Patterson, Distal femur defects reconstructed with polymethylmethacrylate and internal fixation devices: a biomechanical study, Orthopedics 32 (8) (2009) 561–567.

[58] A. Asavamongkolkul, A. Pongkunakorn, T. Harnroongroj, Stability of subchondral bone defect reconstruction at distal femur: comparison between polymethylmethacrylate alone and steinmann pin reinforcement of polymethylmethacrylate, J. Med. Assoc. Thail. 86 (7) (2003) 626–633.

[59] M. Weiner, T.A. Damron, F.R. Patterson, F.W. Werner, K.A. Mann, Biomechanical study of pins in cementing of contained proximal tibia defect, Clin. Orthop. Relat. Res. 419 (2004) 232–237.

[60] J. Ruskin, P. Caravaggi, K.S. Beebe, S. Corgan, L. Chen, R.S. Yoon, F.R. Patterson, J.S. Hwang, Steinmann pin augmentation versus locking plate constructs, J. Orthop. Traumatol. (2016) 1–6.

[61] [cited 2019 June 6th]. Available from: www.tumorlibrary.com.

[62] J. Keyak, I. Lee, D. Nath, H. Skinner, Postfailure compressive behavior of tibial trabecular bone in three anatomic directions, J. Biomed. Mater. Res. 31 (3) (1996) 373–378.